

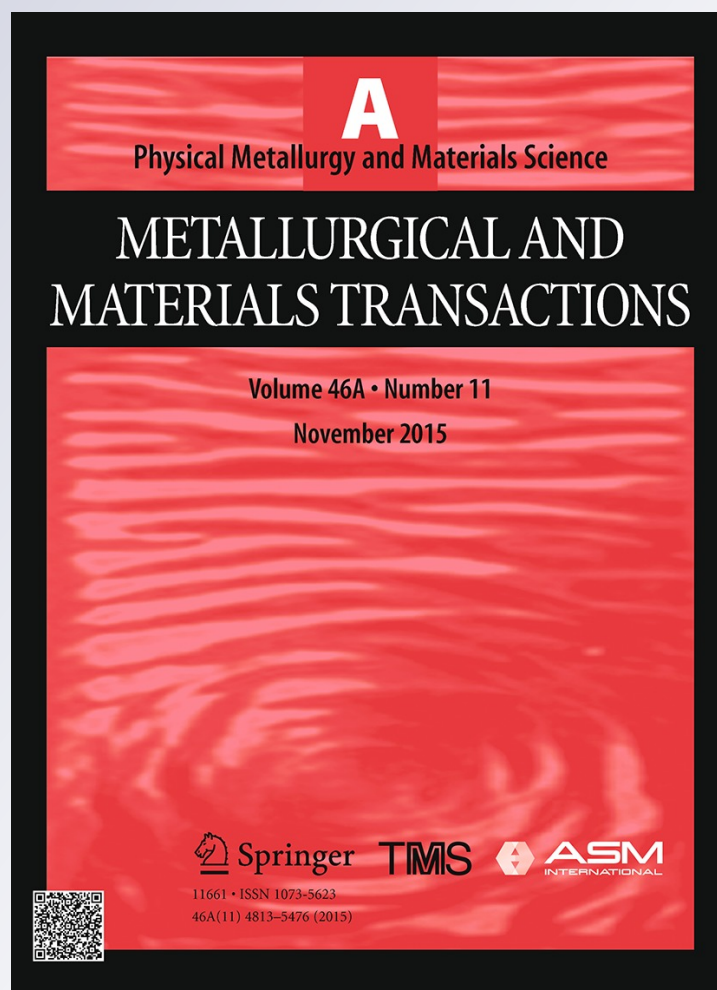
Kinetics of Solute Partitioning During Intercritical Annealing of a Medium-Mn Steel

**H. Kamoutsi, E. Gioti, Gregory
N. Haidemenopoulos, Z. Cai & H. Ding**

**Metallurgical and Materials
Transactions A**

ISSN 1073-5623
Volume 46
Number 11

Metall and Mat Trans A (2015)
46:4841-4846
DOI 10.1007/s11661-015-3118-7



Your article is protected by copyright and all rights are held exclusively by The Minerals, Metals & Materials Society and ASM International. This e-offprint is for personal use only and shall not be self-archived in electronic repositories. If you wish to self-archive your article, please use the accepted manuscript version for posting on your own website. You may further deposit the accepted manuscript version in any repository, provided it is only made publicly available 12 months after official publication or later and provided acknowledgement is given to the original source of publication and a link is inserted to the published article on Springer's website. The link must be accompanied by the following text: "The final publication is available at link.springer.com".

Communication

Kinetics of Solute Partitioning During Intercritical Annealing of a Medium-Mn Steel

H. KAMOUTSI, E. GIOTI,
GREGORY N. HAIDEMENOPOULOS,
Z. CAI, and H. DING

The evolution of austenite fraction and solute partitioning (Mn, Al, and C) during intercritical annealing was calculated for a medium-Mn steel containing 11 pct Mn. Austenite growth takes place in three stages. The first stage is growth under non-partitioning local equilibrium (NPLE) controlled by carbon diffusion in ferrite. The second stage is growth under partitioning local equilibrium (PLE) controlled by diffusion of Mn in ferrite. The third stage is shrinkage of austenite under PLE controlled by diffusion of Mn in austenite. During PLE growth, the austenite is progressively enriched in Mn. Compositional spikes evolve early during NPLE growth and broaden with annealing temperature and time.

DOI: 10.1007/s11661-015-3118-7

© The Minerals, Metals & Materials Society and ASM International 2015

The 3rd generation, medium-Mn, and advanced high-strength steels are under intense investigation as a substitute to 1st (low alloy) and 2nd generation (high-Mn) steels. These steels aim at improved combinations of strength and ductility.^[1-4] In medium-Mn steels, the Mn content is reduced, relative to the high-Mn steels, in the range between 3 and 12 pct and the microstructure consists of an ultrafine ferrite-austenite mixture. The transformation-induced plasticity (TRIP) of the retained austenite is responsible for the enhanced formability in these steels. Several processing routes have been developed in order to stabilize the austenite phase for optimum TRIP interactions. For steels containing between 3 and 8 weight pct Mn, the quench and partitioning (Q&P) process has been

proposed.^[5,6] In this process, austenite is stabilized by carbon partitioning from martensite to austenite, the partitioning taking place between the M_s and M_f temperatures. For steels containing 5 to 12 pct Mn, intercritical annealing, following the cold rolling of the martensitic microstructure, is investigated as a means of stabilizing the austenite by carbon and Mn partitioning.^[7-12] The retained austenite fraction and stability depend, therefore, on the intercritical annealing temperature and time.

Solute partitioning during intercritical annealing in medium-Mn steels has been investigated recently. Most of the research work is concerned with experimental determination of austenite volume fraction and composition.^[13-16] Mn partitioning during intercritical annealing has been studied by atom probe tomography^[13,17] and experimental results have been compared with simulation predictions. Mn partitioning has also been studied by TEM^[14,18-20] indicating that partitioning of Mn from ferrite to the austenite is slow. Thorough thermodynamic analyses of solute partitioning during intercritical annealing have been performed^[21,22] indicating the role of alloying elements. However, kinetic analysis of the partitioning process is limited to relatively few alloy systems, 3 pct Mn,^[23] 5 pct Mn^[24,25], and 12.2 pct Mn.^[17] These works considered a specific intercritical annealing temperature and examined the partition of alloying elements at specific stages of annealing. Furthermore, the evolution of composition spikes of the substitutional solutes with annealing temperature and time is not discussed. It is the aim of the present paper to investigate the evolution of the austenite volume fraction, solute partitioning, and composition spikes during intercritical annealing of as-quenched martensite as a function of annealing temperature and time in a medium-Mn steel.

The experimental medium-Mn steel had a nominal composition (in weight pct) of Fe-0.18C-11Mn-3.8Al. The selected composition was based on the role of alloying elements and an equilibrium thermodynamic analysis that was discussed in recent work.^[11] A 40 kg experimental steel ingot was cast after melting the steel in a vacuum induction furnace. The ingot was heated at 1473 K (1200 °C) for 2 hours, hot forged into rods of section size 100 mm × 30 mm, and then air cooled to room temperature (RT). Subsequently, the rods were soaked at 1473 K (1200 °C) for 2 h, hot-rolled to 4 mm thick strip, and finally air cooled to room temperature (RT). The as-hot-rolled strips were then cold-rolled to 1 mm in thickness. Intercritical annealing was carried out at temperatures in the range of 1003 K to 1123 K (730 °C to 850 °C) for 3 minutes, followed by immediate quenching in water. For metallographic investigation, the samples were etched with 25 pct sodium bisulfite aqueous solution. The microstructures were also examined by scanning electron microscope (SEM). Austenite volume fraction was determined by X-ray

H. KAMOUTSI, Researcher, E. GIOTI, Student, and GREGORY N. HAIDEMENOPOULOS, Professor, are with the Department of Mechanical Engineering, University of Thessaly, Pedion Areos, 38500 Volos, Greece. Contact e-mail: hggreg@mie.uth.gr Z. CAI and H. DING, Professors, are with the School of Materials and Metallurgy, Northeastern University, Shenyang 110819, China.

Manuscript submitted March 4, 2015.

Article published online September 1, 2015

diffraction (XRD) based on the integrated intensities of $(200)\alpha$, $(211)\alpha$, $(200)\gamma$, $(220)\gamma$, and $(311)\gamma$ diffraction peaks.^[21,22]

The austenite formation and associated solute partitioning during intercritical annealing were simulated with the DICTRA software^[26] using the TCFE6 thermodynamic database and the MOBFE2 mobility database for ferrous alloys. A single cell planar geometry was employed, Figure 1(a), with a domain size equal to $1.55\mu\text{m}$. This size corresponds to one-half the measured ferrite-to-austenite mean distance (center to center), as depicted in the micrograph of Figure 1(b). A thin austenite slice, 50 nm size, was attached to the left of the ferrite region. The two regions were discretized with a linear grid possessing a higher density of grid points at the interface. The initial compositions of the austenite slice and ferrite regions were taken equal to the nominal alloy composition. The initial conditions in terms of compositions, in weight pct (W_C , W_{Al} , and W_{Mn}), and activities (a_C , a_{Al} , a_{Mn}) are also depicted in Figure 1(a). Although the compositions in the two phases are identical, the respective activities are not. Diffusional fluxes are generated between the two phases as a response to the activity gradients. Zero flux boundary conditions (closed system) for all elements were imposed at the lower ($x = 0$) and upper ($x = 1.55 \times 10^{-6}$ m) boundaries of the system. Throughout the simulation local equilibrium (LE) conditions were imposed.

The experimental validation of the simulations will be presented first, followed by the evolution of solute partitioning. A comparison between measured and calculated austenite volume fractions as a function of annealing temperature is depicted in Figure 2. The annealing time is 3 min in all cases. The upper curve

in the figure corresponds to the amount of austenite forming at the intercritical annealing temperature. The amount of austenite, which remains after quenching to room temperature, was calculated by subtracting the martensite formed during quenching by employing the Koistinen-Marburger relation^[27]

$$f_M = 1 - \exp[-0.011(M_s - T)],$$

where M_s is the martensite start temperature, the composition dependence of which was recently presented in Reference 28 as

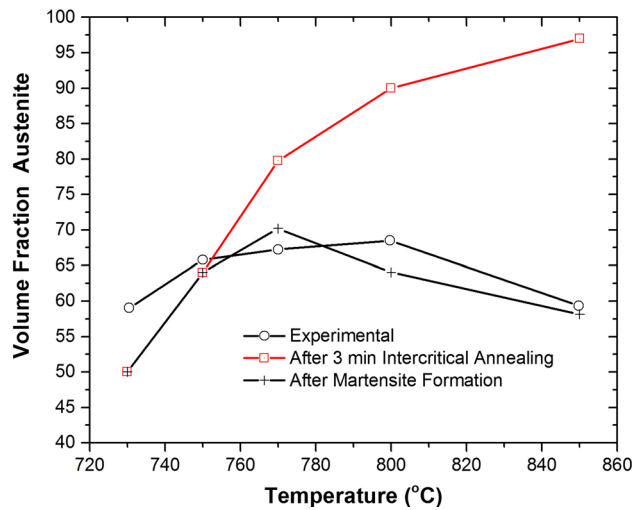


Fig. 2—Volume fraction austenite as a function of annealing temperature for 3 min annealing time. Comparison of calculated values with experimental data.

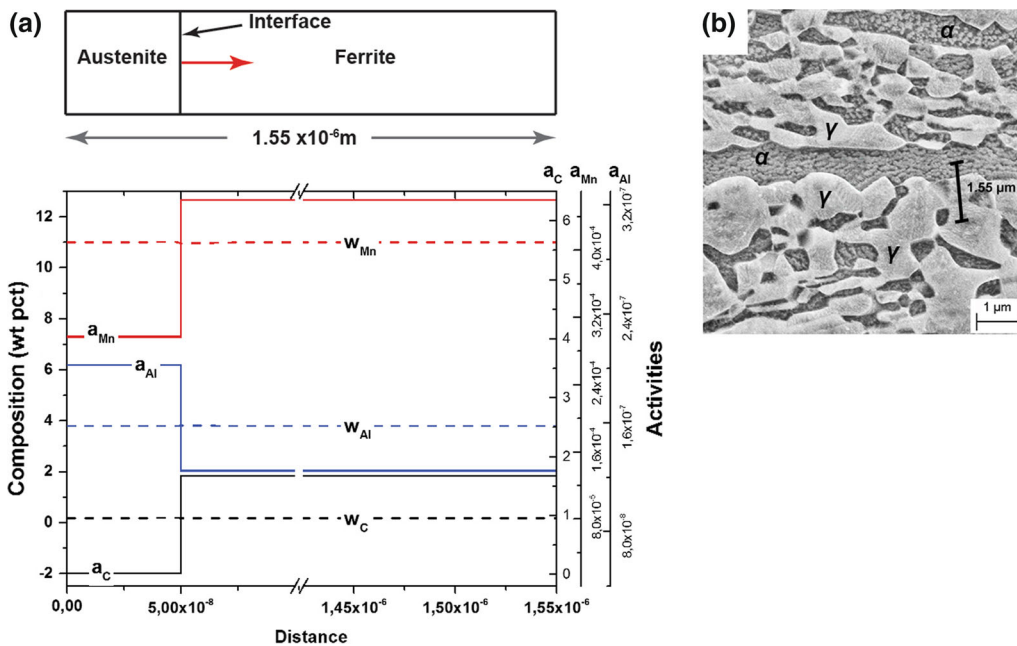


Fig. 1—Simulation domain and initial conditions implemented in DICTRA: (a) initial composition and activity profiles for Mn, Al, and C, (b) SEM micrograph of specimen intercritically annealed at 1023 K (750 °C) indicating the representative domain size for the calculations.

$$M_s = 545 - 601.2[1 - \exp(-0.868C)] - 34.4Mn - 13.7Si - 9.2Cr - 17.3Ni - 15.4Mo + 10.8V + 4.7Co - 1.4Al - 16.3Cu - 361Nb - 2.44Ti$$

In the above relation, the compositions of the elements are in weight pct. The compositions for the calculation of the M_s temperature were the mean compositions of the solute profiles (C, Mn, and Al) in austenite after 3 min annealing time, as calculated by DICTRA. The agreement between the calculated and measured volume fractions is good. This allows the implementation of the method for the computational

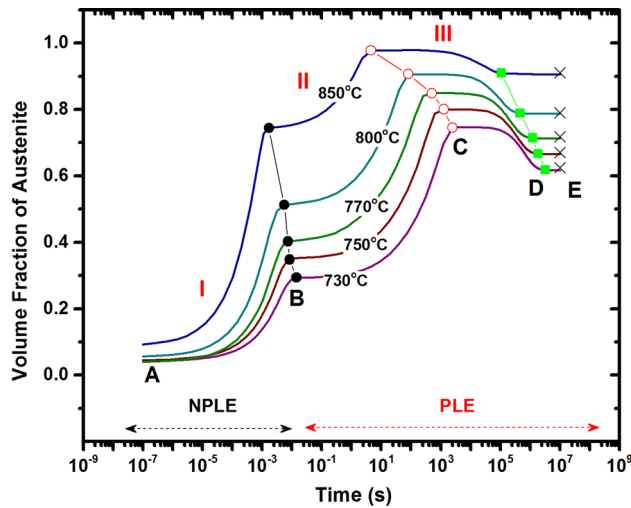


Fig. 3—Evolution of austenite volume fraction with annealing time for several intercritical annealing temperatures, indicating the stages of NPLE and PLE growth.

investigation of solute partitioning during the intercritical annealing of the steel.

The evolution of the volume fraction of austenite during intercritical annealing is depicted in Figure 3 for several annealing temperatures and consists of three stages. In stage I, the initial rapid increase of austenite fraction is due to growth under no-partitioning local equilibrium conditions (NPLE mode), where the growth is controlled by carbon diffusion. In stage II, the intermediate slow growth of austenite is controlled by Mn diffusion in ferrite and takes place under local equilibrium with partition of Mn and Al (PLE mode). In stage III, the final very slow equilibration is controlled by Mn diffusion in austenite and is associated with the shrinkage of austenite. Points B in Figure 3 indicate the NPLE to PLE transition, for each annealing temperature. Points C mark the maximum austenite volume fraction, corresponding to the transition between PLE growth controlled by diffusion of Mn in ferrite and PLE growth controlled by Mn diffusion in austenite. Points D mark the final stable volume fraction of austenite corresponding to the equilibrium volume fractions computed by Thermo-Calc (points E). Similar transformation stages have also been reported in References 23, 24 With increasing the intercritical annealing temperature, the aforementioned transitions take place at shorter times. It is important to note that the amount of austenite formed under NPLE relative to that formed under PLE depends on the annealing temperature. The higher the annealing temperature, the higher the fraction of austenite formed under NPLE mode. In addition, the higher the annealing temperature, the shorter the equilibration stage, and the lower the excess austenite over the equilibrium amount. Solute partitioning during intercritical annealing is presented for each stage below.

Solute partitioning in the NPLE region (stage I) is depicted in Figures 4(a) through (c) for Mn, Al, and carbon for 1023 K (750 °C) annealing temperature and times between 1 × 10⁻⁶ and 1 × 10⁻¹ seconds. The

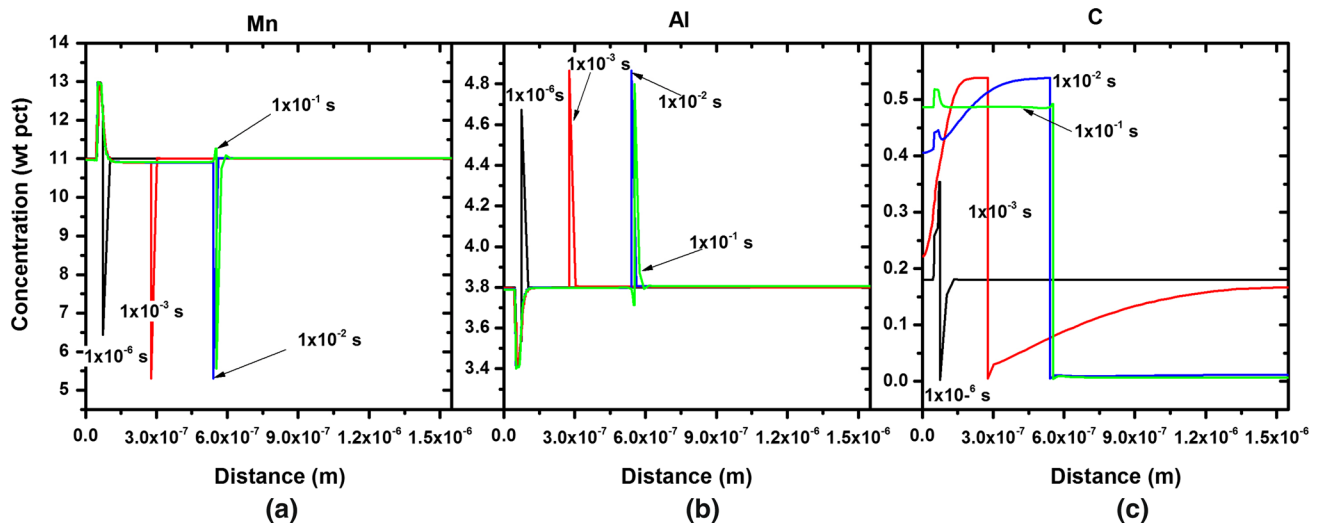


Fig. 4—Profiles of (a) Mn, (b) Al and (c) carbon, after intercritical annealing at 1023 K (750 °C) for the times indicated in the NPLE region of austenite growth (stage I). The austenite and ferrite regions, for each annealing time, are on the left and right of the interface, respectively.

negligible partitioning of Mn results in constant Mn in the two phases, except from a spike of Mn, which forms due to the local equilibrium conditions imposed. The height of the Mn spike at 13 pct is determined by the tie line defined by the intersection of the $\gamma/\alpha + \gamma$ phase boundary with the isoactivity line for carbon in austenite.^[29] Similar Mn spikes have been reported^[13,30] for steels containing 1.7 and 3 pct Mn, respectively. A corresponding 'negative spike' (solute depletion) is exhibited in the Al profile, as well as a carbon spike in the carbon profile. The behavior of these compositional spikes will be discussed in detail later. As stated above, the Mn content in both austenite and ferrite is constant due to NPLE mode up to time $t = 1 \times 10^{-2}$ seconds. For longer times, Mn starts to diffuse from ferrite to austenite. Therefore the NPLE to PLE transition is at $t = 1 \times 10^{-2}$ seconds for the annealing temperature of

1023 K (750 °C). Similar behavior holds for Al. Growth of austenite under NPLE is controlled by carbon diffusion in ferrite. The carbon profile in ferrite is homogenized at $t = 9 \times 10^{-3}$ seconds. In the remaining time up to 1×10^{-2} seconds, the NPLE growth is controlled by carbon diffusion in austenite.

Solute partitioning for Mn, Al, and C is depicted in Figure 5 for the PLE region, stage II, and Figure 6 for the PLE region, stage III. Austenite growth under PLE mode (stage II) is controlled by Mn diffusion in ferrite. There is a significant enrichment of austenite in Mn at the interface with ferrite. This is attributed to the low diffusivity of Mn in austenite, which does not allow the accommodation of the Mn diffusive flux from ferrite. This Mn enrichment of austenite at the interface region has been verified experimentally in a 12.2 pct Mn steel.^[17] Stage II growth takes place up to time

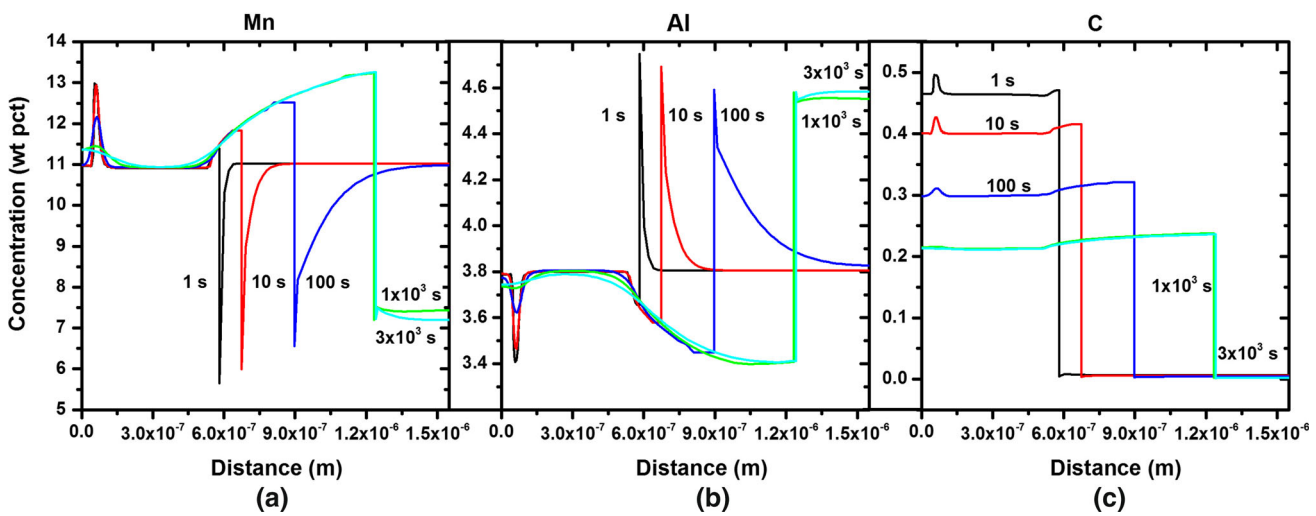


Fig. 5—Profiles of (a) Mn, (b) Al, and (c) carbon after annealing in the PLE region stage II for annealing temperature of 1023 K (750 °C) and the annealing times indicated. The austenite and ferrite regions, for each annealing time, are on the left and right of the interface, respectively.

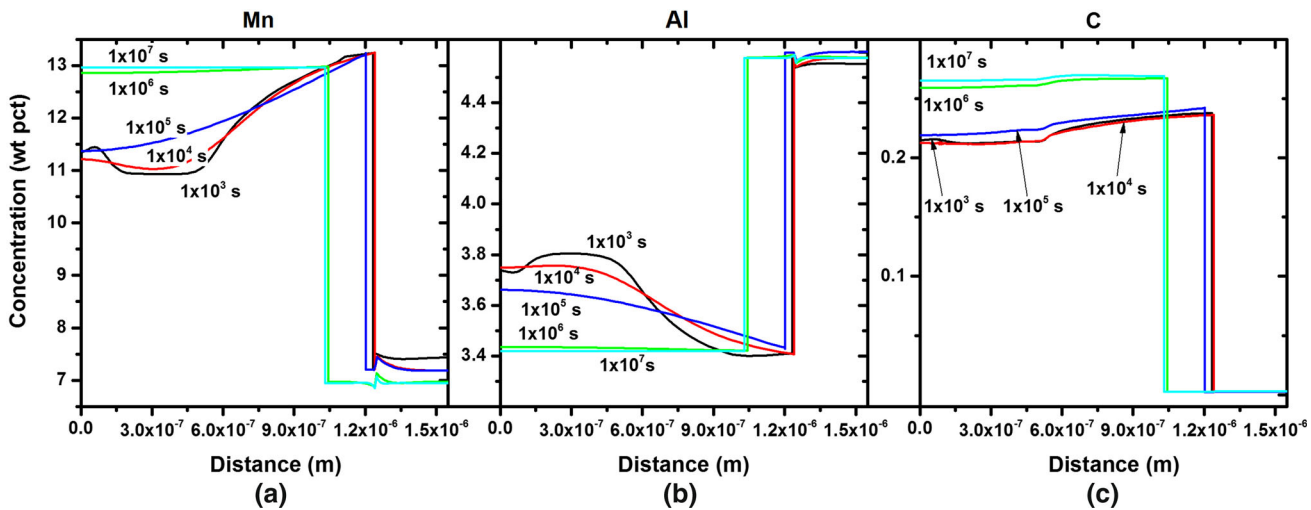


Fig. 6—Profiles of (a) Mn, (b) Al, and (c) carbon after annealing in the PLE region stage III, for annealing temperature of 1023 K (750 °C) and the annealing times indicated. The austenite and ferrite regions, for each annealing time, are on the left and right of the interface, respectively.

$t = 3 \times 10^3$ seconds where the interface stops. As stated above, at this time the austenite volume fraction reaches a maximum value (point C in Figure 3). Thus the transition between PLE stage II and PLE stage III is at $t = 3 \times 10^3$ seconds. During stage III, the interface remains stagnant up to time $t = 10^5$ seconds, and then migrates to the reverse direction corresponding to shrinkage of austenite. The Mn profile in ferrite is homogenized and austenite shrinkage is controlled by Mn diffusion in austenite. At very long times, above $t = 10^6$ seconds, the Mn profile becomes homogeneous in both ferrite and austenite. It is important to note that the Mn profile in austenite is not homogenized during stage II. Homogenization of Mn in austenite takes place at very long times during the shrinkage of austenite (stage III). Al follows a similar behavior. The carbon content in austenite decreases during PLE growth in stage II up to $t = 3 \times 10^3$ seconds. During PLE stage III, where the austenite shrinks, the carbon in austenite increases again and reaches a value about 0.26 pct at very long times, when equilibrium is approached.

The time evolution of the compositional spikes for Mn, Al, and C are depicted for the three stages of intercritical annealing at 1023 K (750 °C) in Figures 7(a) through (i). The Mn spike forms very early in the NPLE region (stage I) due to the LE conditions imposed at the interface, Figure 7(a). The spike width determined from the composition profile of Mn in Figure 7(b) is

0.5×10^{-9} m. A respective value of 1×10^{-9} m has also been reported^[13] for a 1.7 pct Mn steel. Al develops a 'negative spike' in austenite as it diffuses from austenite to ferrite. The evolution of the spikes in PLE stage II, is characterized by broadening with annealing time, as depicted in Figures 7(b), (e), and (h). The spikes are homogenized in PLE stage III, as shown in Figures 7(c), (f), and (i). The effect of annealing temperature for Mn and Al spikes is shown in Figure 8(a) through (d). Two annealing times were considered, $t = 1 \times 10^{-4}$ seconds and $t = 1 \times 10^{-1}$ seconds corresponding to the NPLE and PLE modes of austenite growth, respectively. In both modes, spike broadening takes place with increasing the intercritical annealing temperature.

In summary, the evolution of austenite volume fraction during intercritical annealing takes place in three stages, (I) NPLE growth controlled by carbon diffusion in ferrite, (II) PLE growth controlled by diffusion of Mn in ferrite, and (III) PLE shrinkage of austenite controlled by diffusion of Mn in austenite. The transition from NPLE to PLE mode of growth takes place at shorter times with increasing the annealing temperature. Also the amount of austenite forming under NPLE relative to that forming under PLE increases with the annealing temperature. During PLE growth, the austenite is progressively enriched in Mn but the Mn profile in austenite is homogenized at very long times, during austenite shrinkage in stage III. Compositional spikes evolve very early

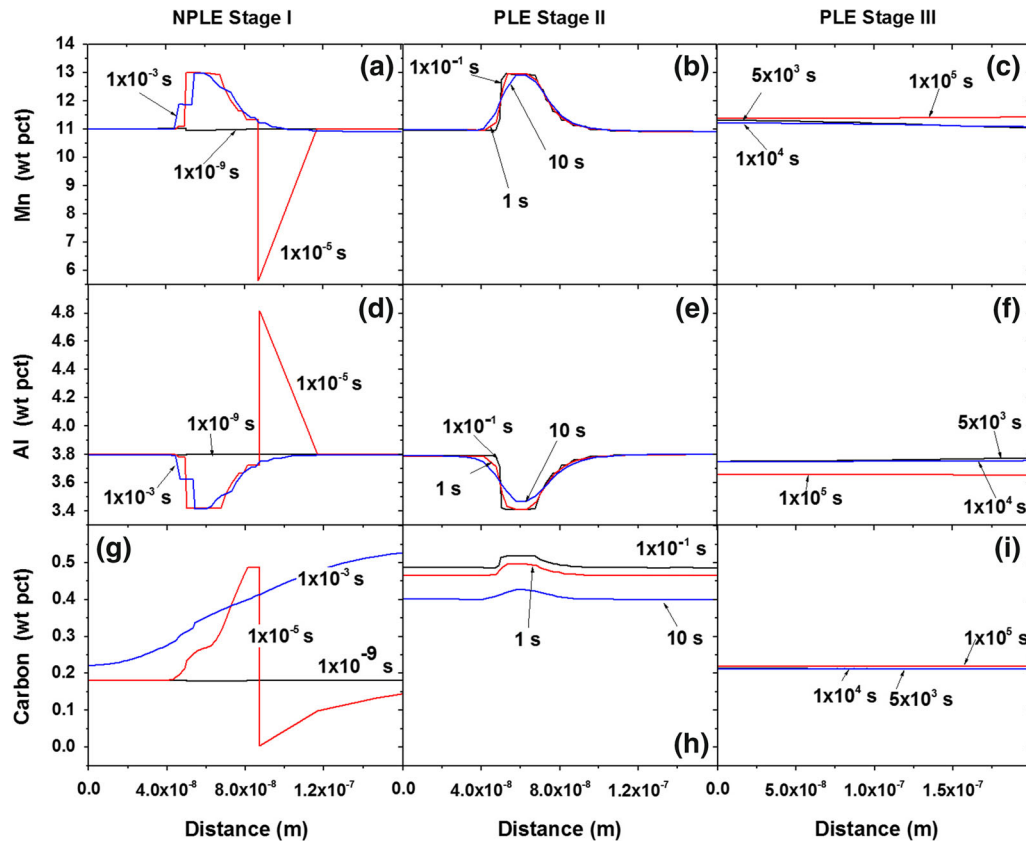


Fig. 7—Evolution of compositional spikes of Mn (a–c), Al (d–f), and carbon (g–i) during intercritical annealing for the three stages of austenite growth and the annealing times indicated.

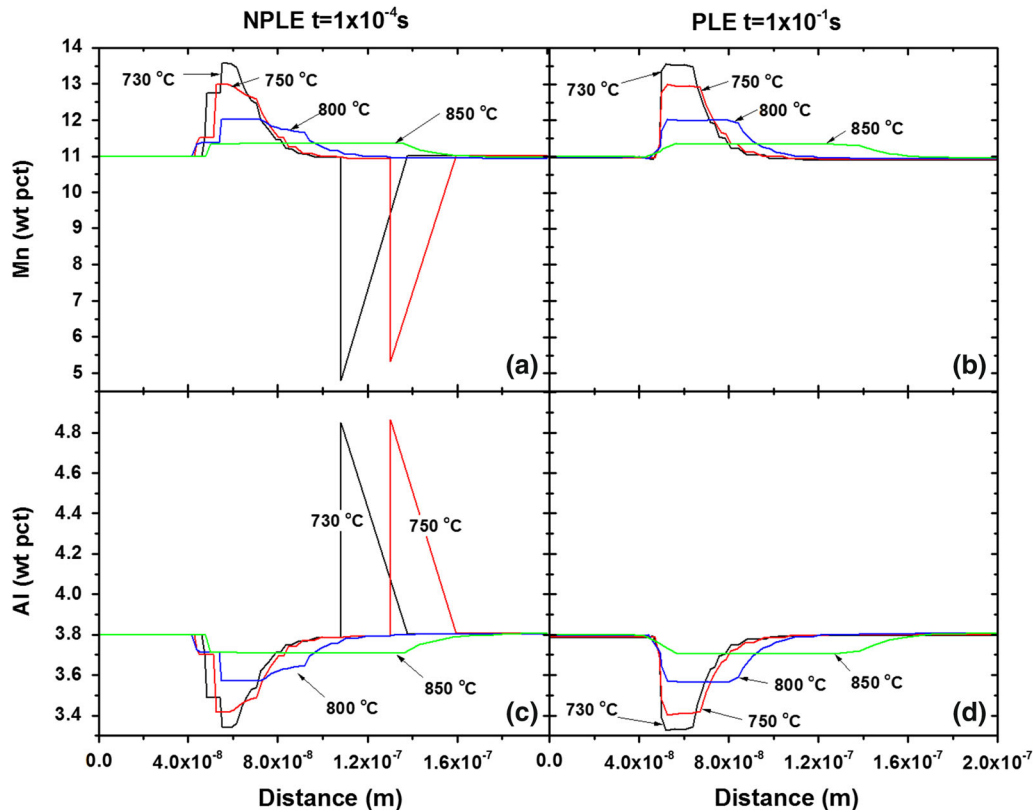


Fig. 8—Effect of annealing temperature on the compositional spikes of Mn (a, b) and Al (c, d) for two different annealing times corresponding to NPLE growth ($t = 1 \times 10^{-4}$ s) and PLE growth ($t = 1 \times 10^{-1}$ s).

during NPLE growth. These spikes broaden with annealing temperature and time.

REFERENCES

1. D.K. Matlock and J.G. Speer: in *Microstructure and Texture in Steels*, A. Haldar, S. Suwas, and D. Bhattacharjee, eds., Springer, London, 2009, pp. 185–205.
2. D.K. Matlock, J. Speer, E. De Moor, and P.J. Gibbs: *JESTECH*, 2012, vol. 15, pp. 1–12.
3. D.W. Suh, J.H. Ryu, M.S. Joo, H.S. Yang, K. Lee H.K.D.H. Bhadeshia: *Metall. Mater. Trans. A*, 2012, vol. 44A, pp. 286–93.
4. S.-J. Lee, S. Lee, and B.C. De Cooman: *Scripta Mater.*, 2011, vol. 64, pp. 649–52.
5. J.G. Speer, F.C.R. Assunção, D.K. Matlock, and D.V. Edmonds: *Mater. Res.*, 2005, vol. 8, pp. 417–23.
6. D.V. Edmonds, K. He, F.C. Rizzo, B.C. De Cooman, D.K. Matlock, and J.G. Speer: *Mater. Sci. Eng. A*, 2006, vols. 438–440, pp. 25–34.
7. R.L. Miller: *Metall. Trans.*, 1972, vol. 3, pp. 905–12.
8. D.-W. Suh, S.-J. Park, T.-H. Lee, C.-S. Oh, and S.-J. Kim: *Metall. Mater. Trans. A*, 2010, vol. 41A, pp. 397–08.
9. M.J. Merwin: SAE Technical paper series, No. 2007-01-0336, SAE Int., 2007.
10. H. Huang, O. Matsumura, and T. Furukawa: *Mater. Sci. Technol.*, 1994, vol. 10, pp. 621–26.
11. Z.H. Cai, H. Ding, X. Xue, and Q.B. Xin: *Mater. Sci. Eng. A*, 2013, vol. 560, pp. 388–95.
12. Z.H. Cai, H. Ding, R.D.K. Misra, H. Kong, and H.Y. Wu: *Mater. Sci. Eng. A*, 2014, vol. 595, pp. 86–91.
13. O. Thuillier, F. Danoix, M. Goune, and D. Blavette: *Scripta Mater.*, 2006, vol. 55, pp. 1071–74.
14. C. Zhao, W.Q. Cao, C. Zhang, Z.G. Yang, H. Dong, and Y.Q. Weng: *Mater. Sci. Technol.*, 2014, vol. 30, pp. 791–99.
15. J. Hu, W. Cao, C. Wang, H. Dong, and J. Li: *ISIJ Int.*, 2014, vol. 54, pp. 1952–57.
16. A. Grajcar, P. Skrzypczyk, and D. Wozniak: *Arch. Metall. Mater.*, 2014, vol. 59, pp. 1692–97.
17. O. Dmitrieva, D. Ponge, G. Inden, J. Millán, P. Choi, J. Sietsma, and D. Raabe: *Acta Mater.*, 2011, vol. 59, pp. 364–74.
18. J. Lis and A. Lis: *J. Achiev. Mater. Manuf. Eng.*, 2008, vol. 26, pp. 195–98.
19. Z.Q. Liu, G. Miyamoto, Z.G. Yang, and T. Furuhashi: *Acta Mater.*, 2013, vol. 61, pp. 3120–29.
20. S. Lee, S.-J. Lee, and B.C. De Cooman: *Scripta Mater.*, 2011, vol. 65, pp. 225–28.
21. S. Lee and B.C. De Cooman: *Metall. Mater. Trans. A*, 2013, vol. 44A, pp. 5018–24.
22. S. Kang, E. De Moor, and J.G. Speer: *Metall. Mater. Trans. A*, 2014, vol. 46A, pp. 1005–11.
23. R. Wei, M. Enomoto, R. Hadian, H.S. Zurob, and G.R. Purdy: *Acta Mater.*, 2013, vol. 61, pp. 697–707.
24. N. Nakada, K. Mizutani, T. Tsuchiyama, and S. Takaki: *Acta Mater.*, 2014, vol. 65, pp. 251–58.
25. E. Gioti, H. Kamoutsi, and G.N. Haidemenopoulos: *Proc. 2nd Int. Conf. on High Manganese Steel*, Aachen, 2014, pp. 337–40.
26. J.O. Andersson, T. Helander, L. Höglund, P. Shi, and B. Sundman: *Calphad*, 2002, vol. 26, pp. 273–312.
27. D.P. Koistinen and R.E. Marburger: *Acta Metall.*, 1959, vol. 7, pp. 59–60.
28. D. Barbier: *Adv. Eng. Mater.*, 2014, vol. 16, pp. 122–27.
29. M. Hillert: *Metall. Trans. A*, 1984, vol. 15A, p. 411.
30. H. Chen, K. Zhu, L. Zhao, and S. van der Zwaag: *Acta Mater.*, 2013, vol. 61, pp. 5458–68.